

# Color Tuning and White Light Emission via in Situ Doping of Luminescent Lanthanide Metal–Organic Frameworks

Qun Tang,<sup>†</sup> Shuxia Liu,<sup>\*,†</sup> Yiwei Liu,<sup>†</sup> Danfeng He,<sup>†</sup> Jun Miao,<sup>†</sup> Xingquan Wang,<sup>†</sup>  
Yujuan Ji,<sup>†</sup> and Zhiping Zheng<sup>\*,‡,§</sup>

<sup>†</sup>Key Laboratory of Polyoxometalate Science of the Ministry of Education, College of Chemistry, Northeast Normal University, Changchun, Jilin 130024, China

<sup>‡</sup>Frontier Institute of Science and Technology, Xi'an Jiaotong University, Xi'an, Shaanxi 710054, China

<sup>§</sup>Department of Chemistry, University of Arizona, Tucson, Arizona 85721, United States

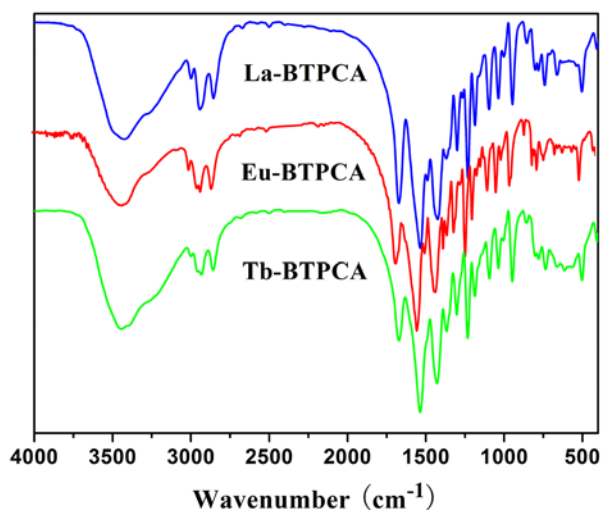


**Figure S1.** IR spectra of **La-BTPCA**, **Eu-BTPCA**, and **Tb-BTPCA**.

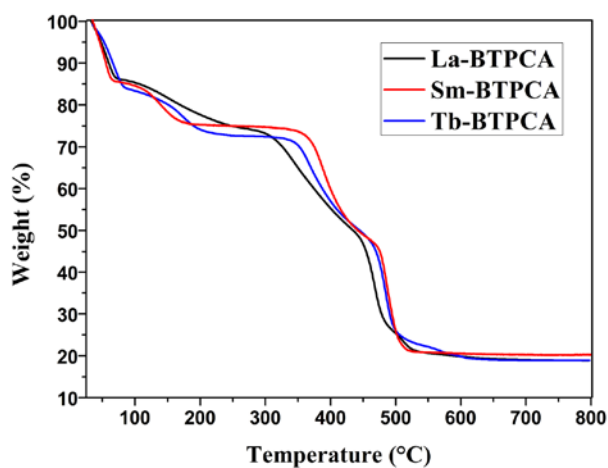


**Figure S2.** Thermogravimetry (TG) curves of the as-synthesized **La-BTPCA**, **Sm-BTPCA**, and **Tb-BTPCA**. Compounds **La-BTPCA**, **Sm-BTPCA**, and **Tb-BTPCA** exhibit similar thermal behavior. The first stage of weight loss was assigned to three water molecules of crystallization and one coordinated water molecules. The second stage of weight loss corresponds to the loss of two DMF molecules of crystallization. The third stage of weight loss corresponds to decomposition of the organic ligands. And final product was  $\text{Ln}_2\text{O}_3$ .

**Table S1.** Elemental analyses (ICP) for **Eu<sub>z</sub>Tb<sub>1-z</sub>-BTPCA**.

Molar ratio of Eu:Tb	Wt% Eu	Wt% Tb
	Calcd (Found)	Calcd (Found)
0.1%: 99.9%	0.10 (0.09)	99.90 (99.91)
0.5%: 99.5%	0.48 (0.55)	99.52 (99.45)
0.75%: 99.25%	0.72 (0.65)	99.28 (99.35)
1.5%: 98.5%	1.44 (1.87)	98.56 (98.13)
3%: 97%	2.87 (2.61)	97.13 (97.39)
5%: 95%	4.79 (4.43)	95.21 (95.57)
7.5%: 92.5%	7.20 (7.54)	92.80 (92.46)
10%: 90%	9.60 (9.82)	90.40 (90.18)

**Table S2.** Elemental analyses (ICP) for **La<sub>x</sub>Eu<sub>y</sub>Tb<sub>1-x-y</sub>-BTPCA**.

Molar ratio of La:Eu:Tb	Wt% La	Wt% Eu	Wt% Tb
	Calcd (Found)	Calcd (Found)	Calcd (Found)
94%: 3%: 3%	93.33 (93.07)	3.26 (3.34)	3.41 (3.59)
70%: 25%: 5%	67.91 (67.66)	26.54 (26.91)	5.55 (5.43)
60%: 10%: 30%	57.00 (57.32)	10.39 (10.19)	32.61 (32.49)
50%: 10%: 40%	46.86 (46.49)	10.25 (10.56)	42.89 (42.95)
45%: 20%: 35%	42.09 (42.46)	20.46 (20.12)	37.45 (37.42)

**Table S3.** Crystal data and structural refinement for compound **Ln-BTPCA** (Ln = La<sup>3+</sup>, Tb<sup>3+</sup>, and Sm<sup>3+</sup>).

Compound	La-BTPCA	Sm-BTPCA	Tb-BTPCA
Formula	C <sub>27</sub> H <sub>49</sub> LaN <sub>8</sub> O <sub>12</sub>	C <sub>27</sub> H <sub>49</sub> SmN <sub>8</sub> O <sub>12</sub>	C <sub>27</sub> H <sub>49</sub> TbN <sub>8</sub> O <sub>12</sub>
Formula weight (g mol <sup>-1</sup> )	816.63	818.63	836.65
<i>T</i> (K)	293(2)	296 (2)	293(2)
Wavelength (Å)	0.71073	0.71073	0.71073
Crystal system	Monoclinic	Monoclinic	Monoclinic
Space group	P 21/c	P 21/c	P 21/n
<i>a</i> (Å)	16.584(5)	16.6053(4)	16.176(4)
<i>b</i> (Å)	26.705(5)	26.7895(8)	7.948(8)
<i>c</i> (Å)	8.180(5)	8.1163(2)	27.278(6)
$\alpha$ (°)	90	90	90
$\beta$ (°)	101.990(5)	101.127(2)	93.50(3)
$\gamma$ (°)	90	90	90
<i>V</i> (Å <sup>3</sup> )	3556(3)	3542.65(16)	3500.505(6)
<i>Z</i>	4	4	4
<i>D</i> <sub>calc</sub> (g cm <sup>-3</sup> )	1.148	1.173	1.204
$\mu$ (mm <sup>-1</sup> )	1.238	1.694	2.057
<i>F</i> (000)	1232.0	1252.0	1264.0
Goodness-of-fit on <i>F</i> <sup>2</sup>	1.042	1.012	1.040
Final <i>R</i> indices [ <i>I</i> > 2σ( <i>I</i> )]	R <sub>1</sub> <sup>a</sup> = 0.0458, wR <sub>2</sub> <sup>b</sup> = 0.0777	R <sub>1</sub> <sup>a</sup> = 0.0332, wR <sub>2</sub> <sup>b</sup> = 0.0716	R <sub>1</sub> <sup>a</sup> = 0.0511, wR <sub>2</sub> <sup>b</sup> = 0.1384
<i>R</i> indices (all data )	R <sub>1</sub> <sup>a</sup> = 0.0754, wR <sub>2</sub> <sup>b</sup> = 0.0828	R <sub>1</sub> <sup>a</sup> = 0.0558, wR <sub>2</sub> <sup>b</sup> = 0.0733	R <sub>1</sub> <sup>a</sup> = 0.0708, wR <sub>2</sub> <sup>b</sup> = 0.1460

$$^a R_1 = \frac{\sum ||F_o| - |F_c||}{\sum |F_o|}; \quad ^b wR_2 = \left\{ \frac{\sum [w(F_o^2 - F_c^2)^2]}{\sum [w(F_o^2)^2]} \right\}^{1/2}.$$

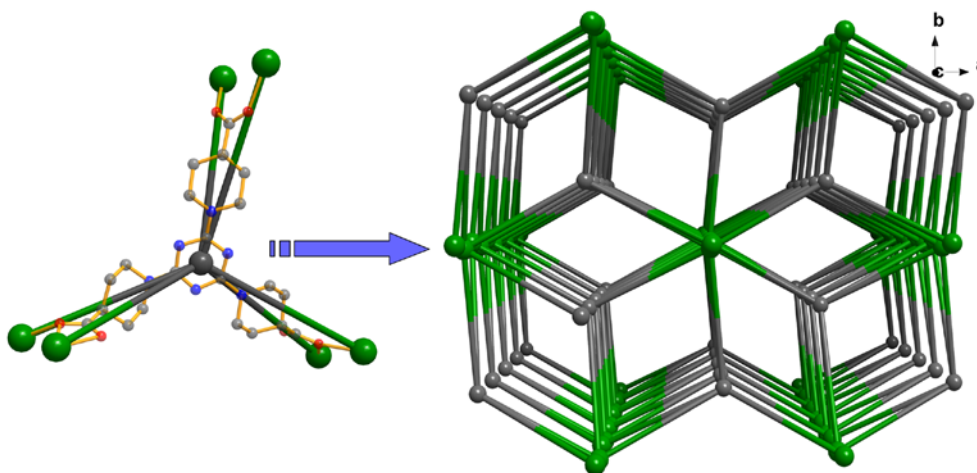


**Figure S3.** The 3D packing and 6, 6-connected net of **Ln-BTPCA** as viewed slightly off the  $c$  axis. The  $\text{Ln}^{3+}$  ion as a six-connected node, and each BTPCA ligand as the other six-connected node. The free solvate molecules and hydrogen atoms were omitted for clarity. TOPOS analysis reveals that this framework is a 6, 6-connected net with point symbol of  $\{4^{12} \cdot 6^3\}\{4^9 \cdot 6^6\}$ . Based on the calculations using PLATON program, the total potential solvent accessible void volume is  $1467.1 \text{ \AA}^3$  and the pore volume ratio is 40.4%.

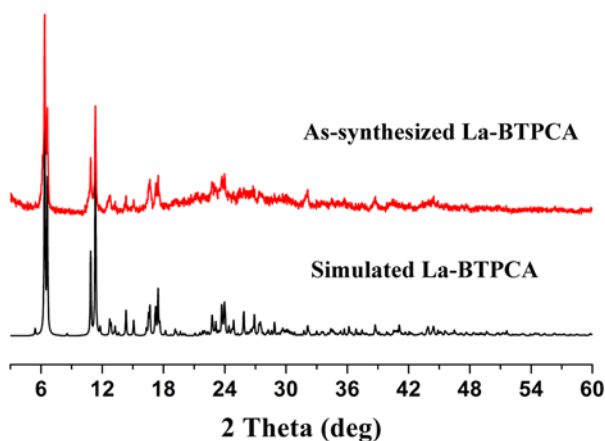


**Figure S4.** Powder X-ray diffraction patterns of simulated **La-BTPCA** and as-synthesized **La-BTPCA**.

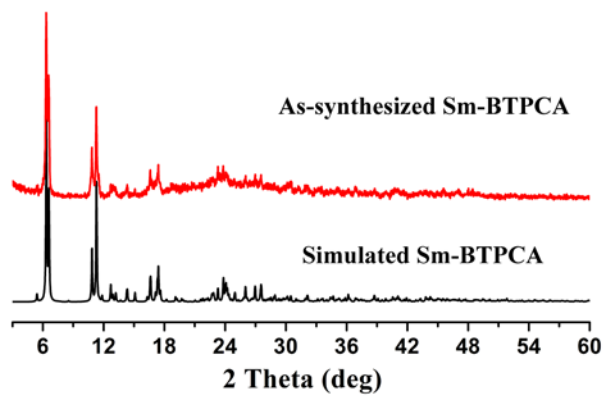


**Figure S5.** Powder X-ray diffraction patterns of simulated **Sm-BTPCA** and as-synthesized **Sm-BTPCA**.

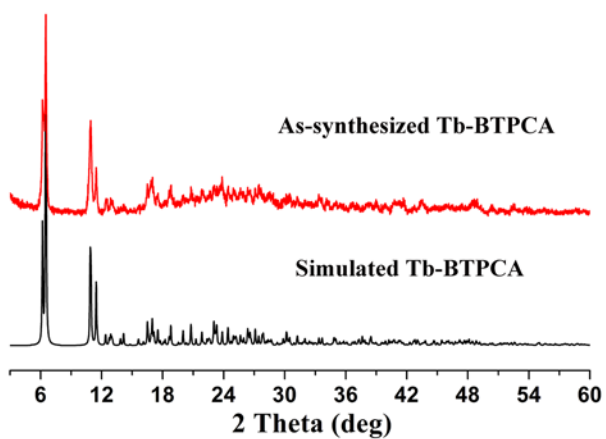


**Figure S6.** Powder X-ray diffraction patterns of simulated **Tb-BTPCA** and as-synthesized **Tb-BTPCA**.

**Table S4.** The unit cell parameters of the **Eu<sub>0.005</sub>Tb<sub>0.995</sub>-BTPCA** and **La<sub>0.6</sub>Eu<sub>0.1</sub>Tb<sub>0.3</sub>-BTPCA** from the single crystal XRD.

Compound	<b>Eu<sub>0.005</sub>Tb<sub>0.995</sub>-BTPCA</b>	<b>La<sub>0.6</sub>Eu<sub>0.1</sub>Tb<sub>0.3</sub>-BTPCA</b>
Crystal system	Monoclinic	Monoclinic
Space group	P 21/c	P 21/n
<i>a</i> (Å)	16.5913(5)	16.166(4)
<i>b</i> (Å)	26.789(6)	7.825(5)
<i>c</i> (Å)	8.137(5)	27.311(6)
$\alpha$ (°)	90	90
$\beta$ (°)	101.921(5)	93.05(3)
$\gamma$ (°)	90	90
<i>V</i> (Å <sup>3</sup> )	3536.88(3)	3519.715(2)

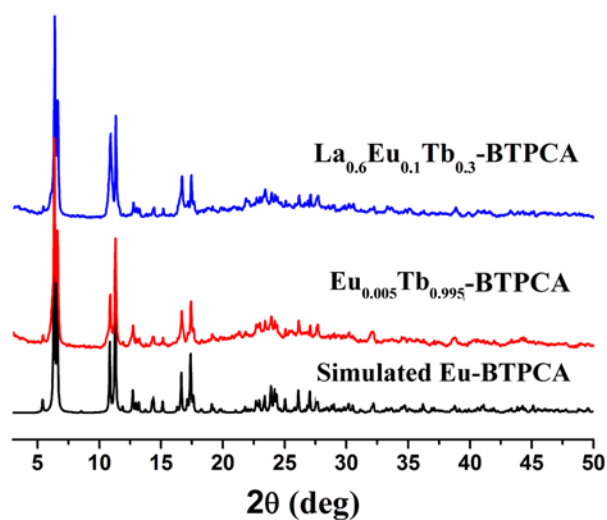


**Figure S7.** Powder X-ray diffraction patterns of simulated **Eu-BTPCA**, as-synthesized **Eu<sub>0.005</sub>Tb<sub>0.995</sub>-BTPCA**, and as-synthesized **La<sub>0.6</sub>Eu<sub>0.1</sub>Tb<sub>0.3</sub>-BTPCA**.

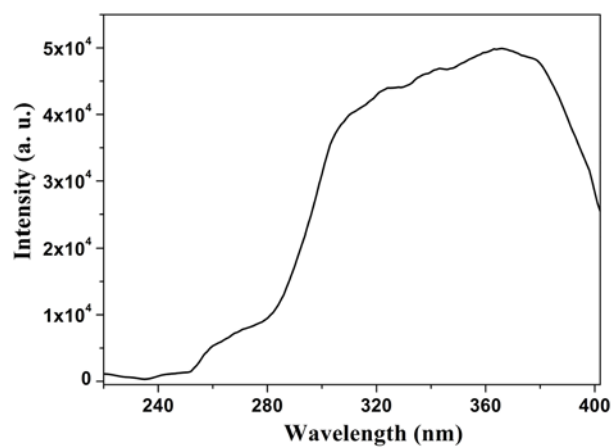


**Figure S8.** The excitation spectrum of **La-BTPCA** upon emission at 445 nm.

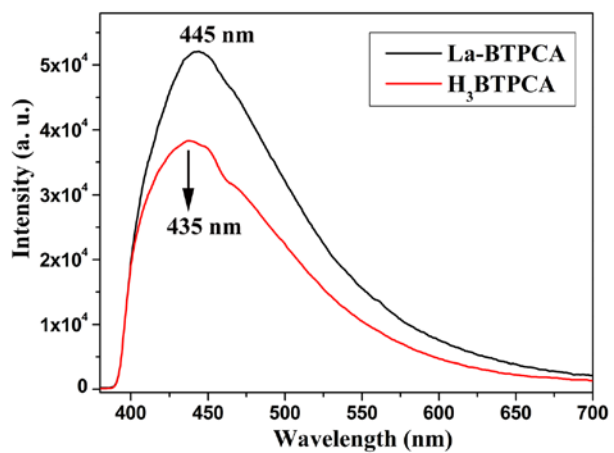


**Figure S9.** The emission spectra of **La-BTPCA** and **H<sub>3</sub>BTPCA** upon excitation at 365 nm.

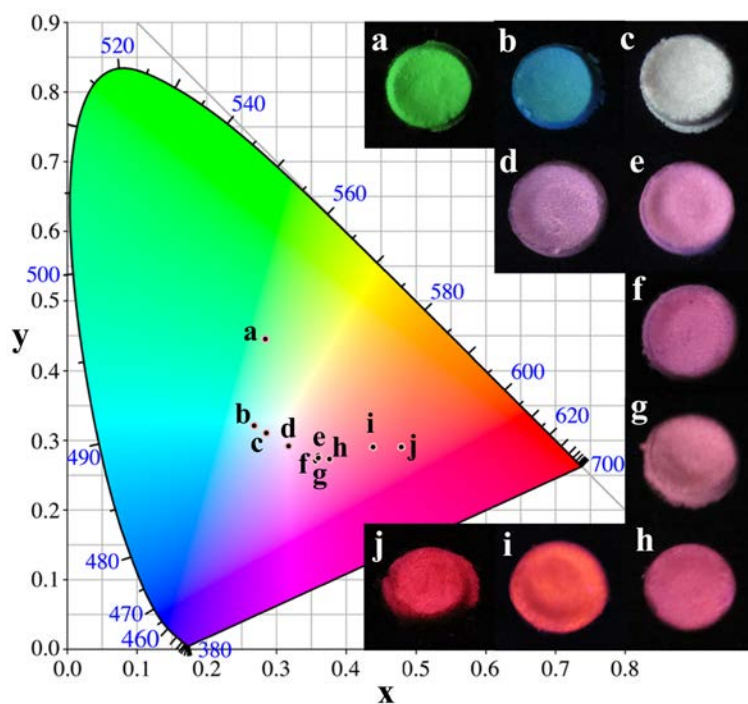


**Figure S10.** The CIE chromaticity coordinates diagram for the  $\text{Eu}_z\text{Tb}_{1-z}\text{-BTPCA}$  ( $z = 0\text{-}100$  mol %) monitored under 365 nm, and the optical photographs excited under 365 nm UV lamps ( $z = 0$  (a), 0.01 (b), 0.1 (c), 0.75 (d), 1.5 (e), 3 (f), 5 (g), 7.5 (h), 10 (i), 100 (j) mol %).

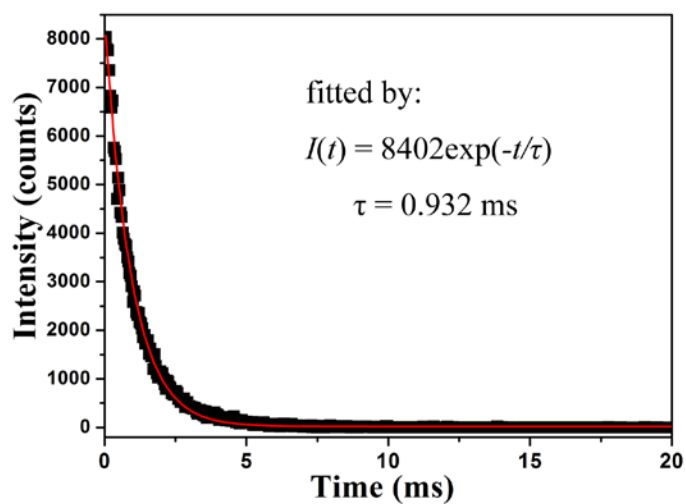


**Figure S11.** The  $^5\text{D}_0$  decay curve of  $\text{Eu-BTPCA}$  recorded at room temperature with emission monitored at 618 nm ( $\lambda_{\text{ex}} = 365$  nm). The red line is the best fit to the data using a mono-exponential function, giving the value of  $\tau = 0.932$  ms.

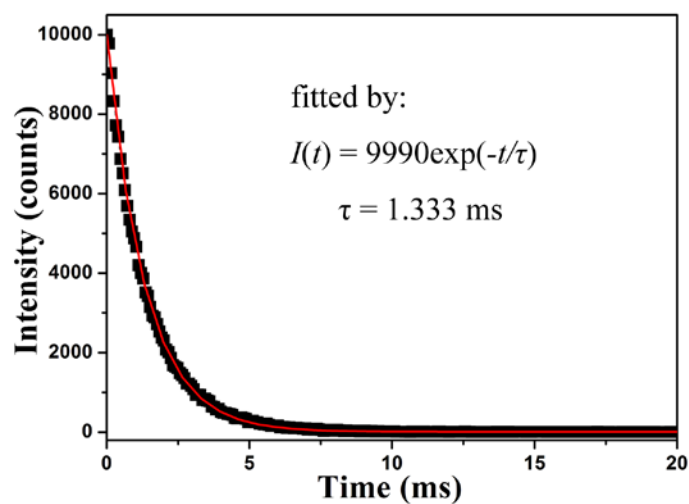


**Figure S12.** The  $^5D_4$  decay curve of **Tb-BTPCA** recorded at room temperature with emission monitored at 545 nm ( $\lambda_{\text{ex}} = 365$  nm). The red line is the best fit to the data using a mono-exponential function, giving the value of  $\tau = 1.333$  ms.

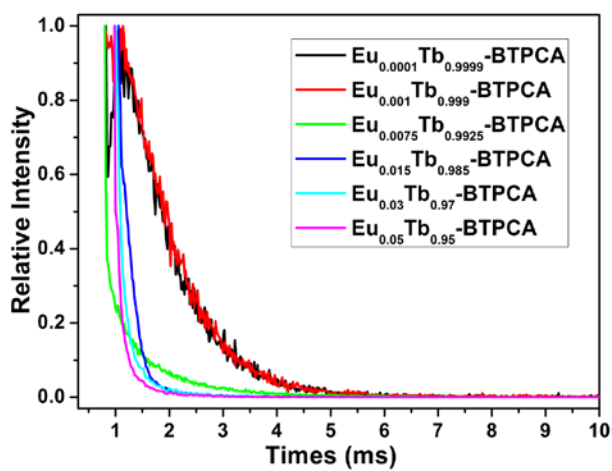


**Figure S13.** The PL decay curve of **Eu<sub>z</sub>Tb<sub>1-z</sub>-BTPCA** ( $z = 0.01\text{--}5$  mol%) recorded at room temperature with emission monitored the  $^5D_4 \rightarrow ^7F_5$  transition at 545 nm ( $\lambda_{\text{ex}} = 365$  nm).

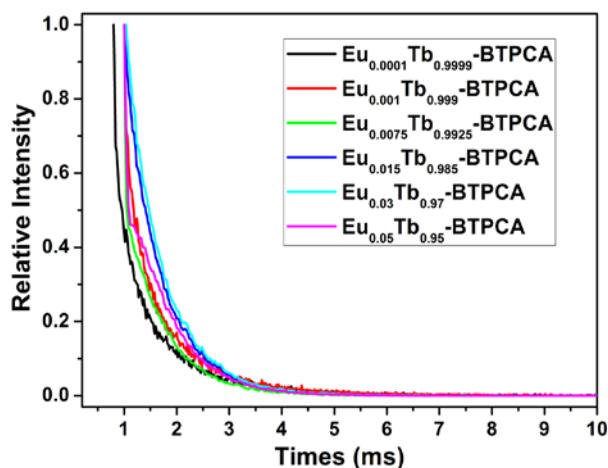


**Figure S14.** The PL decay curve of  $\text{Eu}_z\text{Tb}_{1-z}\text{-BTPCA}$  ( $z = 0.01\text{--}5$  mol%) recorded at room temperature with emission monitored by the  ${}^5\text{D}_0 \rightarrow {}^7\text{F}_2$  transition at 618 nm ( $\lambda_{\text{ex}} = 365$  nm).

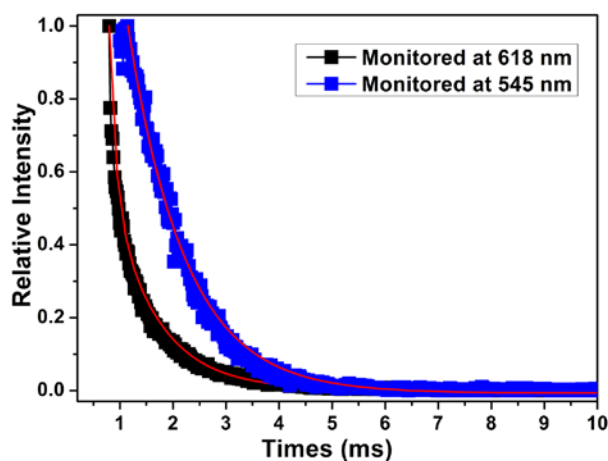


**Figure S15.** The PL decay curve of  $\text{Eu}_{0.005}\text{Tb}_{0.995}\text{-BTPCA}$  recorded at room temperature with emission monitored by the  ${}^5\text{D}_4 \rightarrow {}^7\text{F}_5$  transition at 545 nm and the  ${}^5\text{D}_0 \rightarrow {}^7\text{F}_2$  transition at 618 nm ( $\lambda_{\text{ex}} = 365$  nm). The red lines are the best fit to the data using a mono-exponential function, giving the values of  $\tau_{\text{Tb}^{3+}} = 1.072$  ms, and  $\tau_{\text{Eu}^{3+}} = 0.592$  ms.

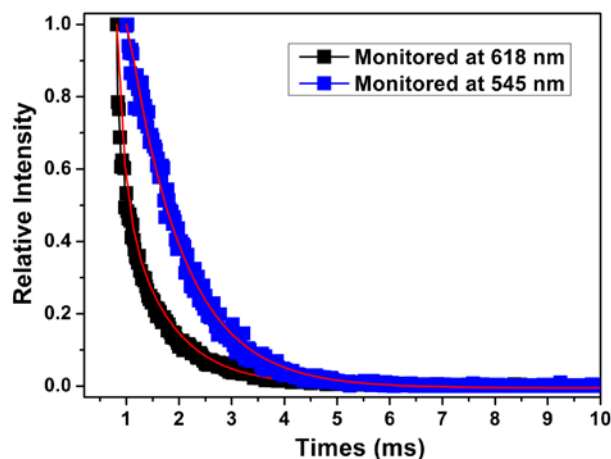


**Figure S16.** The PL decay curve of  $\text{La}_{0.6}\text{Eu}_{0.1}\text{Tb}_{0.3}\text{-BTPCA}$  recorded at room temperature with emission monitored by the  ${}^5\text{D}_4 \rightarrow {}^7\text{F}_5$  transition at 545 nm and the  ${}^5\text{D}_0 \rightarrow {}^7\text{F}_2$  transition at 618 nm ( $\lambda_{\text{ex}} = 365$  nm). The red lines are the best fit to the data using a mono-exponential function, giving the values of  $\tau_{\text{Tb}^{3+}} = 1.027$  ms, and  $\tau_{\text{Eu}^{3+}} = 0.594$  ms.

**Table S5.** CIE chromaticity coordinates for the  $\text{La-BTPCA}$  doped with  $\text{Eu}^{3+}$  and  $\text{Tb}^{3+}$  of different molar ratio excited at 365 nm.

Molar ratio of $\text{La}^{3+}:\text{Eu}^{3+}:\text{Tb}^{3+}$	CIE chromaticity coordinates
94%: 3%: 3%	(0.2124, 0.2228)
70%: 15%: 15%	(0.2572, 0.2554)
70%: 25%: 5%	(0.2983, 0.2527)
70%: 20%: 10%	(0.3991, 0.3000)
60%: 25%: 15%	(0.342, 0.2885)
60%: 35%: 5%	(0.3699, 0.2813)
55%: 20%: 25%	(0.2572, 0.2554)
50%: 25%: 25%	(0.3555, 0.3302)
50%: 15%: 35%	(0.3699, 0.3177)
50%: 10%: 40%	(0.2887, 0.3107)
45%: 20%: 35%	(0.318, 0.3934)

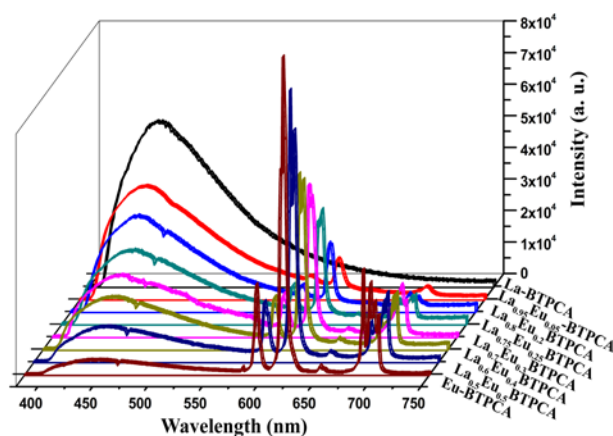


**Figure S17.** Emission spectra of the  $\text{La}_x\text{Eu}_{1-x}\text{-BTPCA}$  ( $x = 0\text{--}100$  mol%) solid samples under 365 nm excitation. The emission spectra exhibit the typical fluorescence peaks of  $\text{Eu}^{3+}$  ions at 591, 617, 650, and 698 nm, which are assigned to the  ${}^5\text{D}_0 \rightarrow {}^7\text{F}_J$  ( $J = 1\text{--}4$ ) transitions of  $\text{Eu}^{3+}$ , and the peak at 445 nm is the ligand-to-metal charge transfer. With the increase of  $\text{Eu}^{3+}$  ion concentration, the luminescent intensity of the  $\text{Eu}^{3+}$  ions increases, and the luminescent intensity of BTPCA decrease.

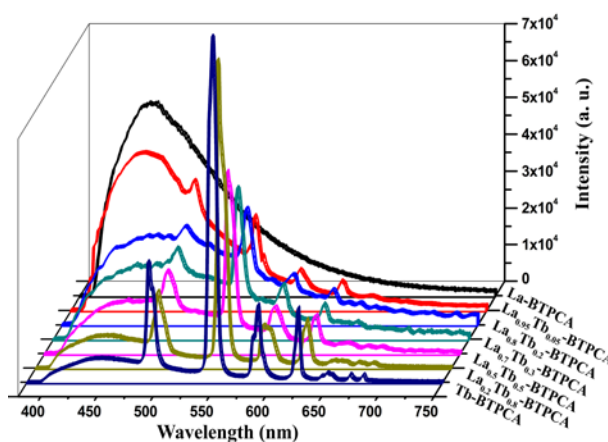


**Figure S18.** Emission spectra of the  $\text{La}_y\text{Tb}_{1-y}\text{-BTPCA}$  ( $y = 0\text{--}100$  mol%) solid samples under 365 nm excitation. The characteristic transitions of  $\text{Tb}^{3+}$  are assigned to transitions between the first excited state ( ${}^5\text{D}_4$ ) and the ground multiplet ( ${}^7\text{F}_J$ ,  $J = 6\text{--}2$ ) at 489, 545, 585, 621, and 648 nm for  $\text{Tb}^{3+}$  in addition to the emission at 445 nm from the BTPCA ligand. With the increase of  $\text{Tb}^{3+}$  ion concentration, the luminescence of the  $\text{Tb}^{3+}$  ions increases, and the emission peaks of  $\text{Tb}^{3+}$  are stronger than the emission of BTPCA ligands.

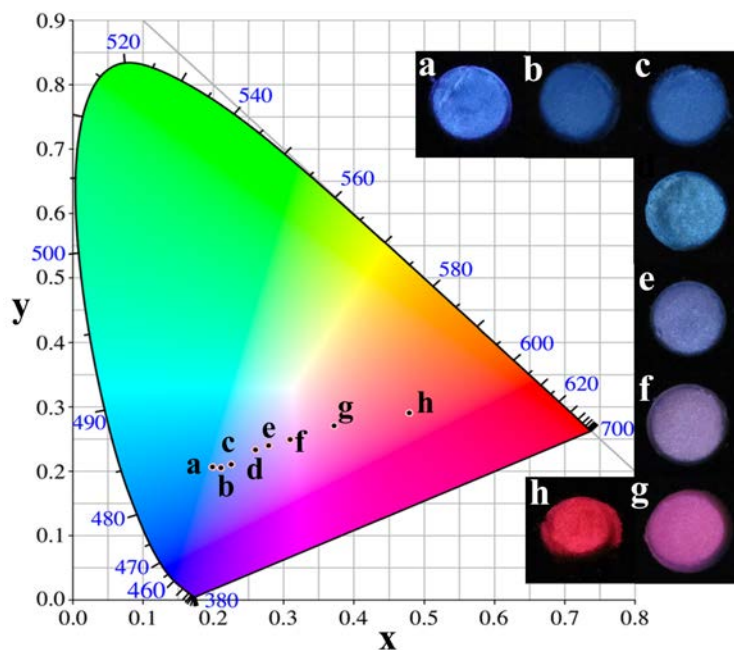


**Figure S19.** The CIE chromaticity coordinates diagram for the  $\text{La}_x\text{Eu}_{1-x}\text{-BTPCA}$  ( $x = 0\text{-}100$  mol%) monitored under 365 nm, and the optical photographs excited under 365 nm UV lamps ( $x = 0$  (a), 5 (b), 20 (c), 25 (d), 30 (e), 40 (f), 50 (g), 100 (h) mol%).

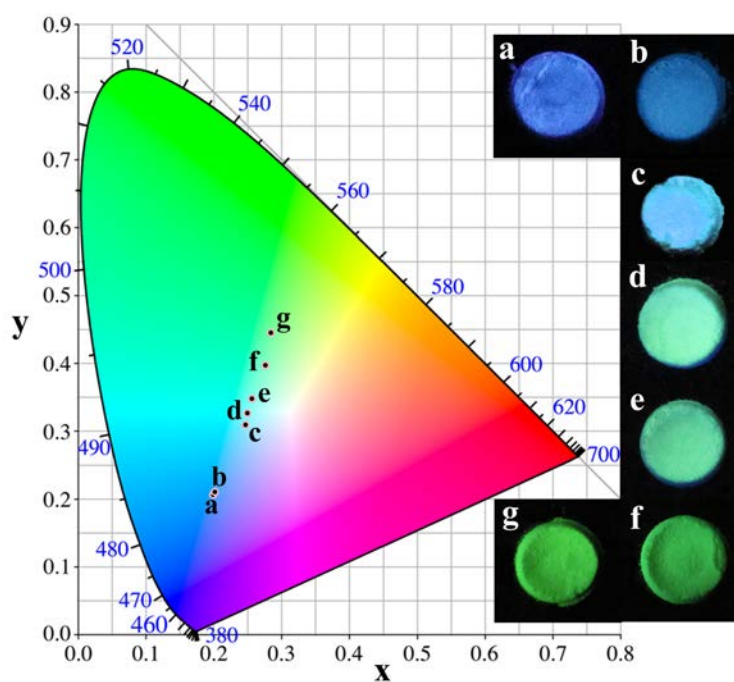


**Figure S20.** The CIE chromaticity coordinates diagram for the  $\text{La}_y\text{Tb}_{1-y}\text{-BTPCA}$  ( $y = 0\text{-}100$  mol%) monitored under 365 nm, and the optical photographs excited under 365 nm UV lamps ( $y = 0$  (a), 5 (b), 20 (c), 30 (d), 50 (e), 80 (f), 100 (g) mol%).